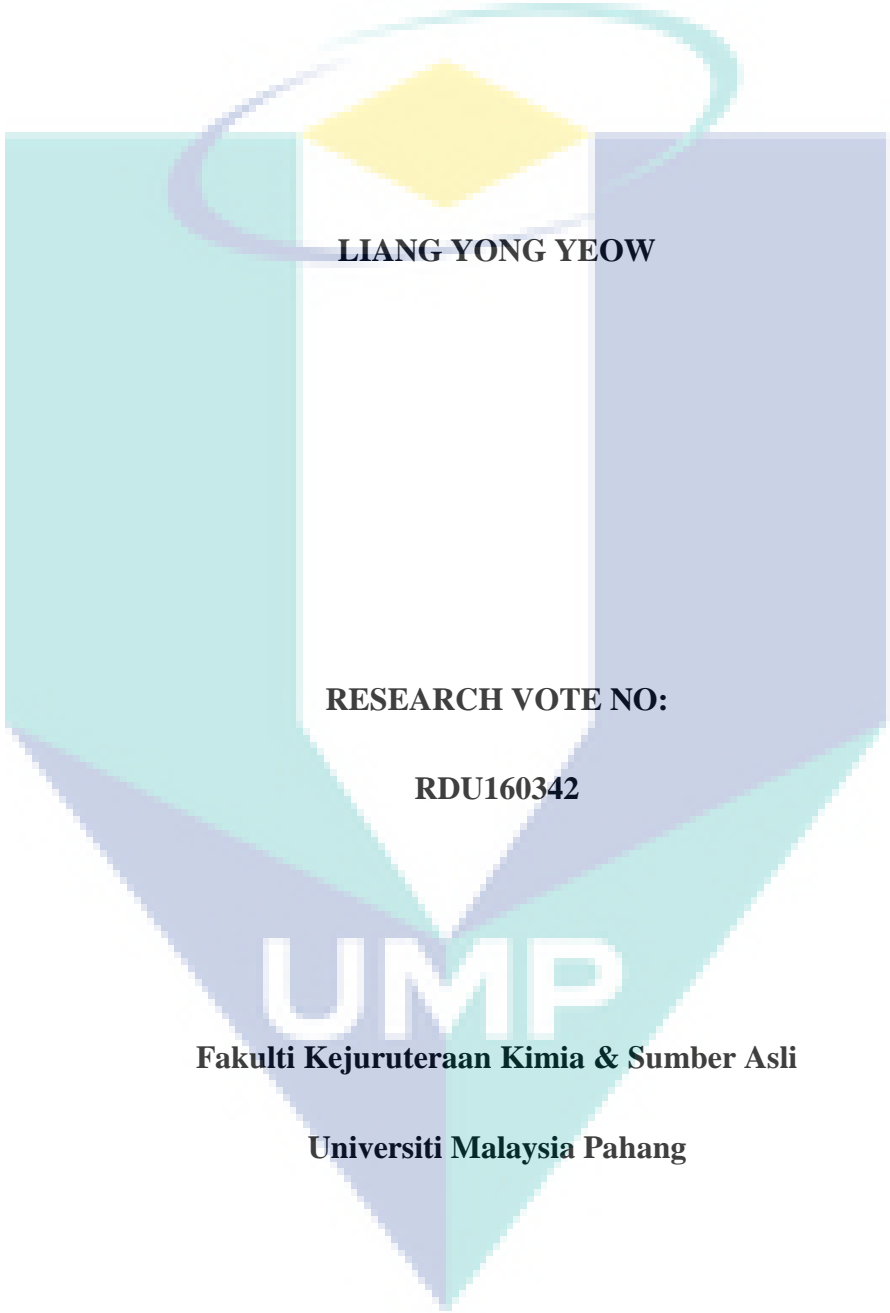


**A CFD STUDY ON THE EFFECT OF MEMBRANE PERMEANCE ON  
PERMEATE FLUX ENHANCEMENT GENERATED BY UNSTEADY SLIP  
VELOCITY**

The logo of the University of Malaysia Pahang (UMP) is a shield-shaped emblem. It features a central white vertical band with a yellow diamond at the top. The shield is divided into four quadrants by this central band and a horizontal line. The top-left and bottom-right quadrants are light blue, while the top-right and bottom-left quadrants are light purple. A stylized, swirling graphic in shades of blue and purple arches over the top of the shield.

**LIANG YONG YEOW**

**RESEARCH VOTE NO:**

**RDU160342**

**UMP**

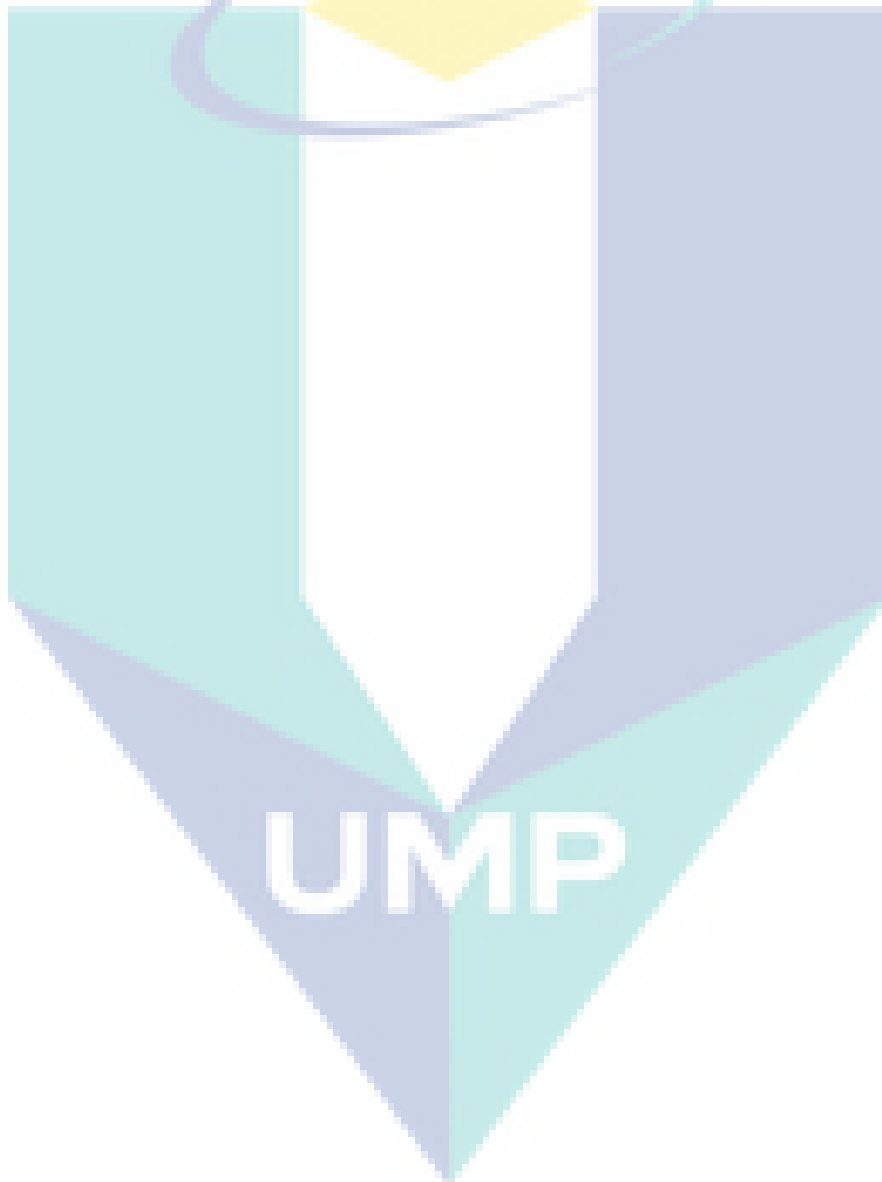
**Fakulti Kejuruteraan Kimia & Sumber Asli**

**Universiti Malaysia Pahang**

**2018**

## DEDICATION

The authors acknowledge the funding support by Universiti Malaysia Pahang research grants (Project numbers RDU160342). One of us (S.Y.L.) gratefully acknowledges scholarship funding by Universiti Malaysia Pahang (UMP).



A CFD study on the effect of membrane permeance on permeate flux enhancement generated  
by unsteady slip velocity

*(Keywords: CFD, Forced Slip Velocity, Permeance, Permeate Flux Enhancement,  
Concentration Polarisation)*

One of the most noteworthy achievements in reverse osmosis (RO) efficiency is the improvement in membrane permeance. Although current membranes offer higher permeance (and flux) than older RO membranes, increases in permeate flux are limited by concentration polarisation (CP) and fouling. Therefore, innovation is needed to reduce CP to further increase permeate flux. An unsteady forced slip velocity can disrupt the boundary layer, thus reducing CP. This paper uses Computational Fluid Dynamics (CFD) to analyse the effect of membrane permeance on the resonant frequency for an unsteady forced slip velocity, as well as the resulting mass transfer enhancement. The results show that the resonant frequency of the unsteady forced slip velocity is not affected by the membrane permeance. Although the results show a peak in the mass transfer enhancement factor for permeance values in the range typically used for brackish water, the permeate flux can also be improved for higher membrane permeances (up to 23 %) at the expense of a slightly higher pumping energy (5-7 %).

Key Researchers:

Liang Yong Yeow

Lim Soon Yee

Gustavo Fimbres Weihs

Dianne Wiley

David Fletcher

E-mail: [yongyeow.liang@ump.edu.my](mailto:yongyeow.liang@ump.edu.my)

Tel. No: +609 549 2859

Vote No.: RDU160342

Kajian CFD mengenai kesan permeance membran pada peningkatan aliran fluks yang dihasilkan oleh halaju slip yang tidak stabi

*(Kata kunci: CFD, Halaju Slip Paksa, Permeance, Peningkatan Fluks Permeate, Polarisasi Kepekatan)*

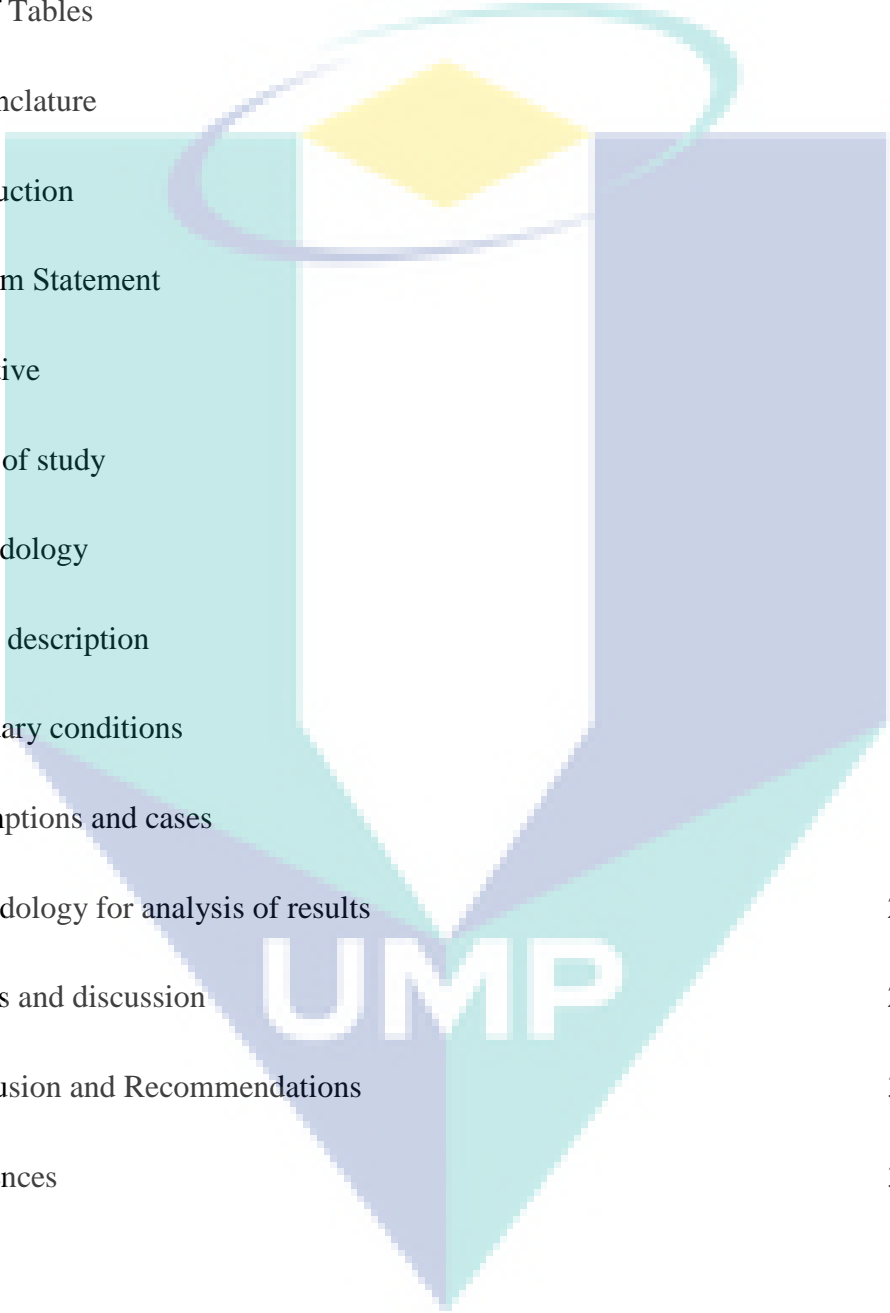
Salah satu pencapaian yang paling penting dalam kecekapan osmosis terbalik (RO) ialah peningkatan permeance membran. Walaupun membran semasa menawarkan permeance yang lebih tinggi (dan fluks) daripada membran RO yang lebih lama, peningkatan dalam fluks dihadkan oleh polarisasi konsentrasi (CP) dan fouling. Oleh itu, inovasi diperlukan untuk mengurangkan CP untuk terus meningkatkan fluks permeate. Halaju slip terpaksa yang tidak stabil boleh mengganggu lapisan sempadan, dengan itu mengurangkan CP. Jurnal ini menggunakan Computational Fluid Dynamics (CFD) untuk menganalisis kesan permeance membran pada frekuensi resonansi untuk halaju slip terpaksa yang tidak stabil, serta peningkatan pemindahan jisim yang terhasil. Keputusan menunjukkan bahawa frekuensi resonansi halaju slip terpaksa yang tidak stabil tidak terjejas oleh permeance membran. Walaupun keputusan menunjukkan puncak peningkatan dalam faktor penambahan pemindahan jisim untuk nilai permeance air payau, fluks permeate juga boleh ditingkatkan untuk permeans membran yang lebih tinggi (sehingga 23%) dengan menggunakan tenaga pam yang sedikit lebih tinggi (5-7%).

Key Researchers:  
Liang Yong Yeow  
Lim Soon Yee  
Gustavo Fimbres Weihs  
Dianne Wiley  
David Fletcher

E-mail: [yongyeow.liang@ump.edu.my](mailto:yongyeow.liang@ump.edu.my)  
Tel. No: +609 549 2859  
Vote No.: RDU160342

## TABLE OF CONTENTS

List of Figures	6
List of Tables	7
Nomenclature	8
1 Introduction	13
1.1 Problem Statement	15
1.2 Objective	15
1.3 Scope of study	16
2 Methodology	17
2.1 Model description	17
2.2 Boundary conditions	19
2.3 Assumptions and cases	19
2.4 Methodology for analysis of results	21
3 Results and discussion	24
4 Conclusion and Recommendations	33
References	35

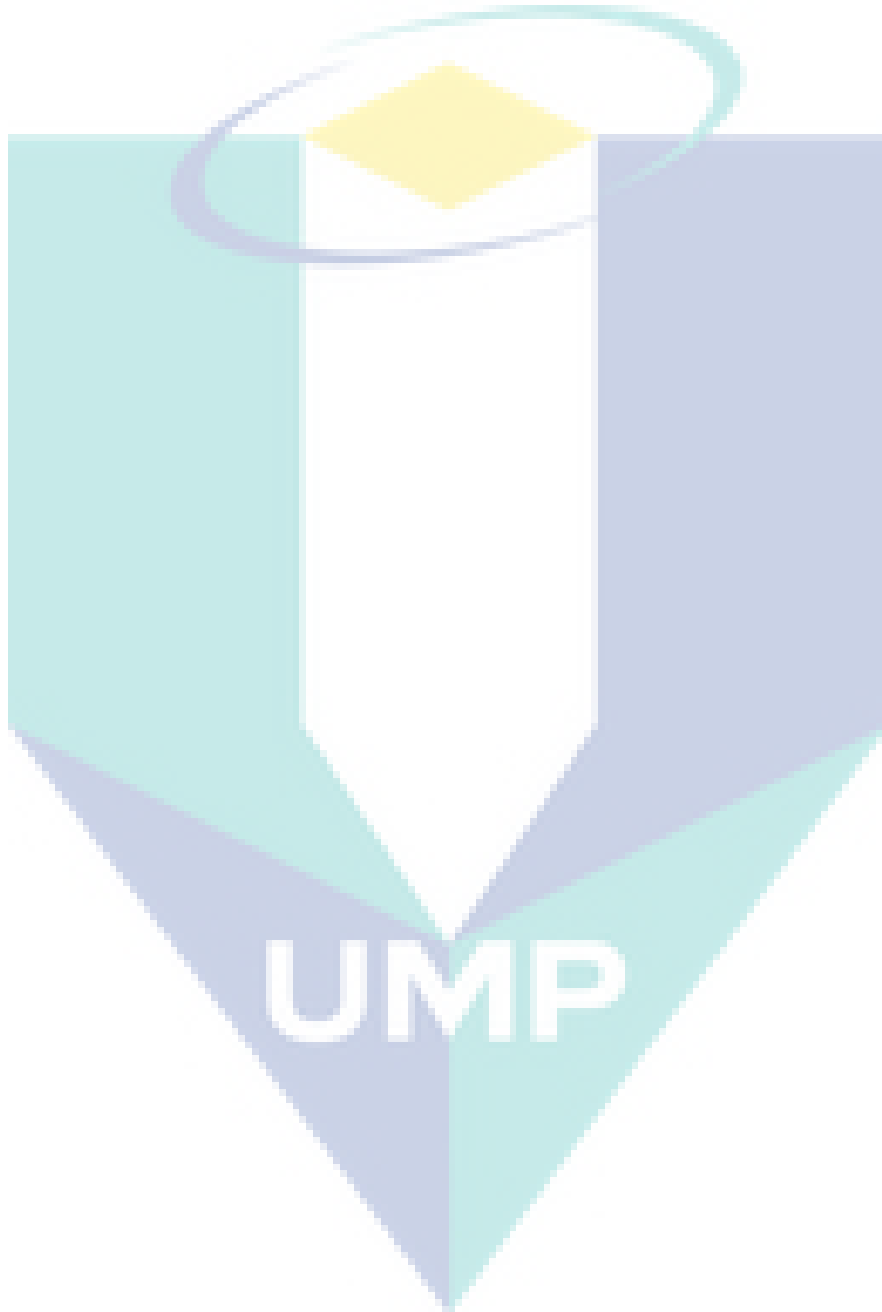


## LIST OF FIGURES

2.1	Schematic of fluid domain (not to scale) indicating boundary locations and channel regions. Red arrows on the membrane surface indicate the location of slip velocity (as in [1]).	17
2.2	Geometry of the spacer unit cell (as in [18]).	17
3.1	Frequency response time data for the pulse slip velocity and corresponding $v$ -velocity at monitoring point ‘•’ (located at one third of the channel height from the bottom membrane surface), for $\Pi_{Lp} = 4.94 \times 10^{-5}$ , $2.21 \times 10^{-4}$ , $8.69 \times 10^{-4}$ and $2.21 \times 10^{-3}$ at the same feed bulk concentration ( $w_{b0} = 0.025$ ) and $Re = 408$ .	25
3.2	Frequency response of $v$ -velocity at location ‘•’ to a pulse in slip velocity for $\Pi_{Lp} = 4.94 \times 10^{-5}$ , $2.21 \times 10^{-4}$ , $8.69 \times 10^{-4}$ and $2.21 \times 10^{-3}$ at the same feed solute concentration ( $w_{b0} = 0.025$ ) and $Re = 408$ .	26
3.3	Effect of membrane permeance on (a) forced slip velocity mass transfer enhancement and (b) relative change in permeate flux at different inlet solute concentration ( $w_{b0}$ ) of 0.01 ( $\Delta p_{tm} = 2.94$ MPa), 0.025 ( $\Delta p_{tm} = 2.94$ MPa) and 0.04 ( $\Delta p_{tm} = 6$ MPa) for $Re = 408$ .	28
3.4	Effect of slip velocity applied at the $F_{peak}$ on the velocity field and solute concentration in the region within spacer 8 for $\Pi_{Lp} = 4.94 \times 10^{-5}$ and $2.21 \times 10^{-3}$ at the same feed solute concentration ( $w_{b0} = 0.025$ ) and $Re = 408$ .	30
3.5	Effect of membrane permeance on (a) maximum shear stress and (b) Power number at three different values of $w_{b0}$ : 0.01 ( $\Delta p_{tm} = 2.94$ MPa), 0.025 ( $\Delta p_{tm} = 2.94$ MPa) and 0.04 ( $\Delta p_{tm} = 6$ MPa) for $Re = 408$ .	31

## LIST OF TABLES

3.1	Parameters used for slip velocity case study	19
3.2	Dimensionless variables used for this study	20



## NOMENCLATURE

*Symbol*

$D$	Solute diffusivity	$\text{m}^2 \text{s}^{-1}$
$d_f$	Filament diameter	m
$d_h$	Hydraulic diameter	m
$E_x$	Electric field in the $x$ -direction	$\text{V m}^{-1}$
$F_{peak}$	Dimensionless actual peak frequency	
$F_{pl}$	Dimensionless peak frequency predicted by frequency response	
$F_s$	Dimensionless frequency of oscillation of slip velocity	
$f$	Friction factor	
$f_{cut}$	Cut-off frequency	$\text{s}^{-1}$
$f_s$	Frequency of oscillation of slip velocity	$\text{s}^{-1}$
$h_{ch}$	Height of channel	m
$J$	Permeate flux	$\text{kg m}^{-2} \text{s}^{-1}$
$J_{pure} = \rho L_p \Delta p_{tm}$	Permeate flux through membrane for a pure water system	$\text{kg m}^{-2} \text{s}^{-1}$
$L_{in}$	Entrance length	m
$L_m$	Membrane length	m
$L_{out}$	Exit length	m
$L_p$	Membrane permeance	$\text{m s}^{-1} \text{Pa}^{-1}$

$l_m$	Mesh length	m
$P_0$	Dimensionless inlet transmembrane pressure	
$p$	Pressure	Pa
$\Delta p_{tm}$	Inlet transmembrane pressure	Pa
$R$	Membrane intrinsic rejection	
$Re_{CR}$	Critical Reynolds number	
$Re_h = \frac{\rho u_{eff} d_h}{\mu}$	Hydraulic Reynolds number	
$Re_s$	Slip Reynolds number	
$t$	Time	s
$U_{s,A}$	Dimensionless forced slip velocity amplitude	
$U_{s,pulse}$	Dimensionless forced slip velocity	
$u$	Local velocity in the $x$ -direction	$m\ s^{-1}$
$u_{eff} = u_{b0}/\varepsilon$	Effective velocity	$m\ s^{-1}$
$u_s$	Slip velocity	$m\ s^{-1}$
$u_{s,A}$	Oscillation amplitude of slip velocity	$m\ s^{-1}$
$v$	Local velocity in the $y$ -direction	$m\ s^{-1}$
$w$	Solute mass fraction	
$w_{ch}$	Membrane channel width	m
$x$	Distance in the bulk flow direction, parallel to membrane surface	m

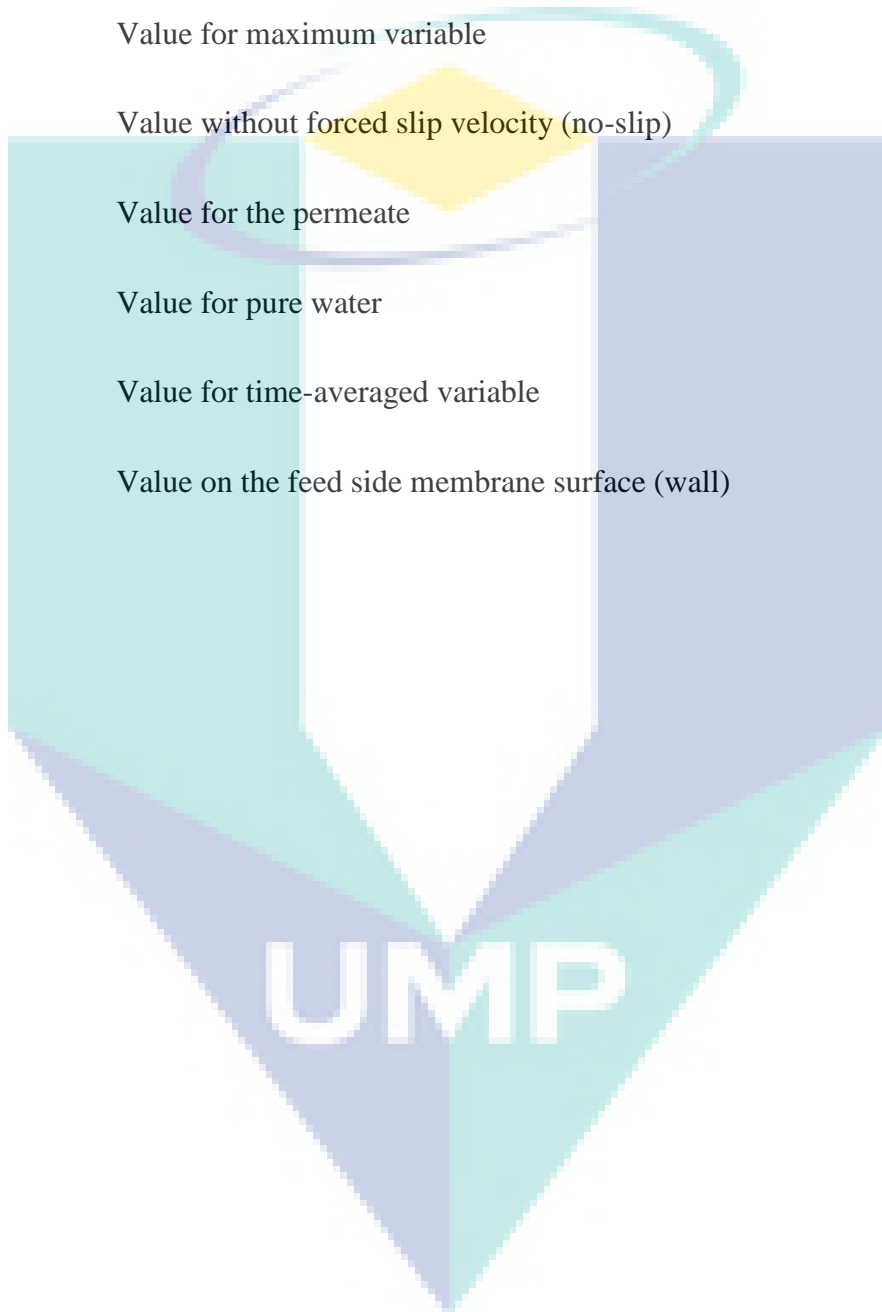
$y$  Distance from the bottom membrane surface, in direction normal to the surface m

*Greek letters*

$\gamma$	Concentration polarisation index (modulus)	
$\varepsilon$	Porosity	
$\varepsilon_e$	Permittivity	F m <sup>-1</sup>
$\zeta$	Zeta potential	V
$\mu$	Dynamic viscosity	kg m <sup>-1</sup> s <sup>-1</sup>
$\pi$	Osmotic pressure	Pa
$\pi_0 = \varphi w_{b0}$	Inlet osmotic pressure	Pa
$\Pi_{Lp}$	Dimensionless membrane permeance	
$\rho$	Fluid density	kg m <sup>-3</sup>
$\sigma$	Reflection coefficient	
$\tau$	Wall shear stress	Pa
$\varphi$	Osmotic pressure coefficient	Pa
$\Phi$	Local mass transfer enhancement factor	
$\tilde{\Phi}$	Global mass transfer enhancement factor	

*Subscript*

<i>b0</i>	Value at inlet bulk conditions
<i>EO</i>	Value with forced slip velocity
<i>max</i>	Value for maximum variable
<i>NS</i>	Value without forced slip velocity (no-slip)
<i>p</i>	Value for the permeate
<i>pure</i>	Value for pure water
<i>TA</i>	Value for time-averaged variable
<i>w</i>	Value on the feed side membrane surface (wall)



## CHAPTER 1

### INTRODUCTION

#### 1 Introduction

Commercial water treatment processes mostly employ spiral wound membrane (SWM) and hollow fibre modules in processes such as desalination, water reclamation and waste water treatment. However, concentration polarisation (CP) is one of the major drawbacks for any membrane module. CP occurs when there is a gradual build-up of non-permeable components in the feed side as more permeable components pass through the membrane. Thus, CP can result in an increase in osmotic pressure, a decrease in permeate flux ( $J$ ), and accelerate the onset of fouling [2-5].

Recently, with advancements in the fields of nanotechnology and biotechnology, scientists and researchers have suggested that ultra-permeable membranes (UPMs) will be the next generation reverse osmosis (RO) membranes for desalination [6, 7]. For instance, a recent study by Cohen-Tanugi et al. [7] shows that a membrane with  $3\times$  higher membrane permeance ( $L_p$ ) yields a reduction of 44–63 % in the number of pressure vessels and capital investment requirements.

One way to create unsteadiness in SWMs is to increase the feed flow rate or Reynolds number beyond a critical Reynolds number ( $Re_{CR}$ ), such that the spacers induce vortex shedding and promote mixing in the laminar flow regime [8]. Various studies have focused on the effect of spacer geometry on mass transfer [9-12], but only a few studies have

explored the effect of spacers in combination with other boundary layer disruption techniques (e.g. forced slip velocity [13], pulsation [14, 15] and vibration [16]) to enhance mixing and increase permeate flux. Those studies have shown that these methods can induce flow perturbations near the boundary layer, which have the potential to enhance membrane performance. Electro-osmotic flow (EOF) is one of the hydrodynamic methods that can be used to generate a forced slip velocity. Under EOF conditions, an applied external electrical field induces an electro-osmotic slip velocity in the vicinity of a charged surface, where it can perturb the flow, promote boundary layer renewal and, therefore, increase mixing and mass transfer [1, 15, 17].

The Helmholtz-Smoluchowski (HS) slip velocity approach can simplify the complex mathematical modelling of EOF within the boundary layer, while maintaining computational accuracy and validity [18]. This is because the component of the electrical field normal to the membrane has negligible effect under typical RO conditions; thus, the HS slip velocity approach only needs to account for the tangential component of the electric field.

A uniform steady slip velocity has been shown [17] to have the potential to reduce flow stagnation and the development of high concentration in the vicinity of spacer filaments. Later work [13] also found synergies for unsteady-state forced slip velocity in spacer-filled channels, which leads to higher mass transfer enhancement than for empty channels. These unsteady results show that there is a resonant frequency (input frequency at which the amplitude of response is largest) that induces vortex shedding, leading to boundary layer renewal and enhanced mass transfer. Moreover, flow pulsations [15] can also induce vortex shedding when applied at the resonant frequency. This suggests that flow perturbation methods applied at the resonant frequency should have the potential to induce vortex shedding.

Although flow perturbations can induce vortex shedding, this only occurs when the oscillating perturbations occur within a specific range of frequencies. If the oscillation frequency is too low, vortex shedding does not occur because the system achieves quasi-steady-state within each perturbation period. If the oscillation frequency is too high, the system does not have time to respond to the perturbation and it behaves as if it were at steady state. In both of these cases, the system dampens the oscillations along the channel. However, when the oscillations are within a specific range, they grow along the channel, eventually causing vortex shedding and increasing mass transfer. Within that range, the maximum mass transfer is achieved at the resonant frequency. Our previous work found that the peak frequency depends on the Reynolds number [13]. It is therefore useful to be able to determine the peak frequency in order to maximise the effect of unsteady forced slip on mass transfer.

## 1.1 Problem Statement

With higher  $L_p$ , concentration polarisation also increases. To address this problem, innovation is needed to reduce CP for membranes with higher  $L_p$ . Such innovation can potentially be achieved by the application of unsteady shear strategies. Unsteady shear strategies have been proven to be superior to a steady-state high shear approach in terms of energy efficiency [19], because boundary-layer renewal reduces concentration polarisation and improves permeate flux.

## 1.2 Objective

- 1) To understand whether forced slip resonant frequency affected by the membrane permeance.

2) To investigate whether membrane permeance affects unsteady mixing in the vicinity of the boundary layer of membrane channels, and to determine if such an approach has the potential to improve the permeate flux, even for high permeance membranes.

### **1.3 Scope of the study**

For numerical studies, validation is of utmost importance to ensure that a model can be relied upon to provide results of practical relevance. The HS model used in our previous work [1, 13, 17, 18] has been thoroughly validated with literature data for conditions under steady and unsteady forced slip velocity. Moreover, experimental tests of the operation schemes analysed in this work would require spatial and temporal resolution approaching (and in some cases surpassing) the capabilities of current visualisation techniques [1]. Hence, direct experimental validation is not included in the scope of this paper, as the purpose of this work is to explore the possible scenarios and identify the most promising operating conditions for a later experimental study of the slip velocity-disturbed boundary layer in a membrane channel. An imposed forced slip is therefore used in this paper to analyse the effect of a flow perturbation velocity located on the membrane surface, its specific effects on the hydrodynamics of the boundary layer, and the overall performance of the membrane system. Although this paper uses an unsteady forced slip velocity to disrupt the boundary layer, it is important to note that this is not the only method that can be used to enhance mass transfer for a membrane system. Other hydrodynamic-based approaches, such as pulsation and vibration methods, can also be used to induce vortex shedding, change the flow in the boundary layer and, thus, improve mass transfer and reduce concentration polarisation.

## CHAPTER 2

### METHODOLOGY

#### 2.1 Model description

Two-dimensional, constant property transient Newtonian fluid flow is simulated inside a narrow spacer-filled membrane channel, using the CFD code ANSYS CFX 16.2, following the method and assumptions of our previous studies [13, 18]. The software package solves the coupled continuity, momentum and mass transfer equations for a given set of initial and boundary conditions. For constant property Newtonian fluid flow, these governing equations are as follows:

$$\nabla \cdot \vec{v} = 0 \quad (1)$$

$$\rho \frac{\partial \vec{v}}{\partial t} + \rho(\vec{v} \cdot \nabla)\vec{v} = \mu \nabla^2 \vec{v} - \nabla p \quad (2)$$

$$\rho \frac{\partial w}{\partial t} + \rho \nabla \cdot (w\vec{v}) = D \nabla^2 w \quad (3)$$

Figure 2.1 and 2.2 illustrate the channel and electrode geometry used in this paper, which is the same geometry as in [20]. Further details on the model parameters are presented in Table 2.1. The region around the unit cell containing spacer 7 and 8 is used for detailed analysis of the local and global variables. In this study, a hydraulic Reynolds number ( $Re_h$ ) of 408 is used for all cases under consideration, as it was previously found to be a flow regime that significantly benefits from the synergies between the spacers and unsteady forced slip

mass transfer enhancement [1]. A Helmholtz-Smoluchowski slip velocity ( $u_s = -\frac{\epsilon_e \zeta E_x}{\mu}$ ) of  $0.5 \text{ mm s}^{-1}$  with an electric field ( $E_x$ ) of the order of  $10^4 \text{ V m}^{-1}$  and a zeta potential ( $\zeta$ ) of the order of  $-10^{-2} \text{ V}$  is used. The slip velocity can be made dimensionless using the fluid density, the hydraulic diameter and the fluid viscosity as  $Re_s = \frac{\rho u_s A d_h}{\mu}$ . The simulations are restricted to 2D flow because 3D simulations require exponentially higher computational resources and time (especially for transient simulations) than that required to simulate 2D flow. Moreover, since geometries similar to that used here do not present significant 3D effects in the Reynolds number range used for this study [21-23], the 3D flow behaviour is not expected to alter the trends in mass transfer behaviour presented in this paper.

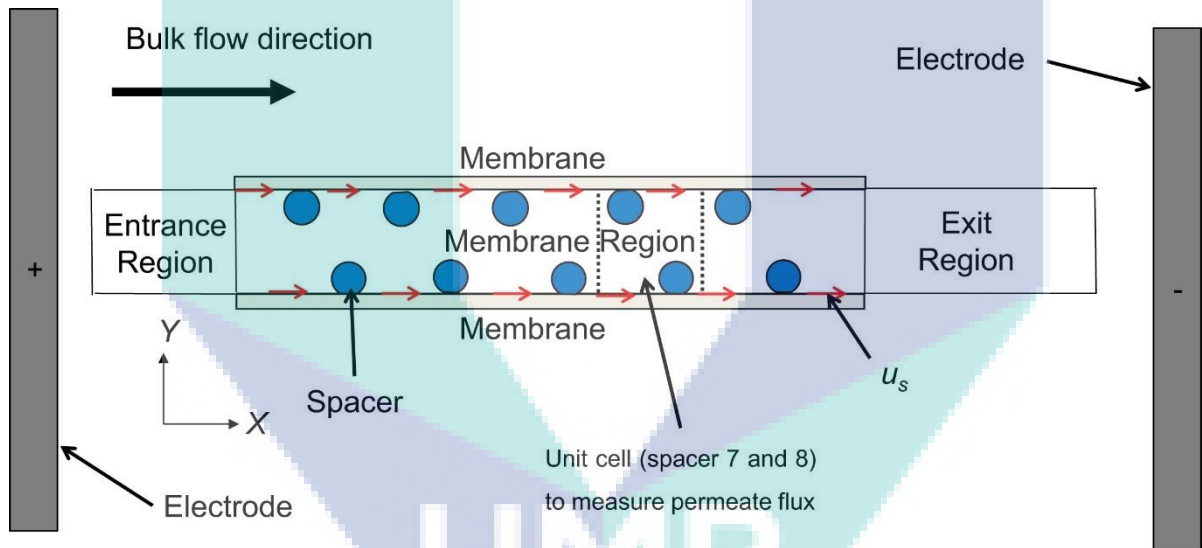


Figure 2.1: Schematic of fluid domain (not to scale) indicating boundary locations and channel regions. Red arrows on the membrane surface indicate the location of slip velocity (as in [1]).

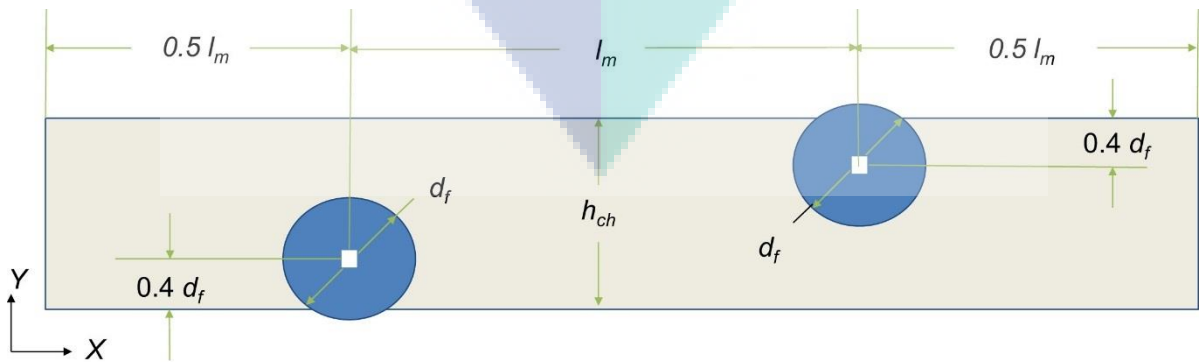


Figure 2.2: Geometry of the spacer unit cell (as in [1]).

## 2.2 Boundary conditions

As in our previous work [13], only the spacer filament surfaces and the channel walls in the entrance and exit regions are treated as non-slip ( $u = v = 0$ ), while the top and bottom walls of the membrane region have non-zero velocity boundary conditions ( $u = u_s$ ,  $v = v_w$  for the top wall and  $v = -v_w$  for the bottom wall). The volumetric flux across the membrane ( $v_w$ ) depends on the local salt concentration, according to the Kedem-Katchalsky-Merten equation [24]:

$$v_w = \frac{J}{\rho} = L_p(\Delta p_{tm} - \sigma\phi R w_w) \quad (4)$$

The CFD calculation determines the solute concentration at the membrane surface based on a flux balance condition [24]. A more detailed description of the permeate flux calculation can be found elsewhere [17]. The slip velocity is implemented in the form of a sinusoidal waveform, which is defined as [25]:

$$U_{s,t} = \frac{u_{s,A}}{u_{eff}} \sin(2\pi f_s t) = U_{s,A} \sin(2\pi f_s t) \quad (5)$$

where  $t$ ,  $f_s$ ,  $u_{eff}$  and  $u_{s,A}$  are time, frequency of oscillation, effective velocity and slip velocity amplitude, respectively.

## 2.3 Assumption and cases

A mesh independence study was carried out to establish the accuracy of the CFD solution. The final mesh discretisation consists of at least 30 elements within an inflation layer normal to all solid boundaries with a thickness equal to approximately 2 % of the channel height, and non-structured elements with a maximum size of 1 % of the channel

height. The mesh used comprised ~2 million elements has a Grid Convergence Index (GCI) below 5 % for both mass transfer and permeate flux, meaning that the mesh resolution is within an acceptable range, and that this potential source of the numerical error can be safely neglected.

Around the world, typical concentrations of dissolved solids in brackish water can range from 1,000 to 10,000 mg/L (mass fraction  $w = 0.001-0.01$ ), while the typical concentrations for seawater are much higher, ranging from around 35,000 mg/L ( $w = 0.035$ ) to greater than 45,000 mg/L ( $w = 0.045$ ) [17]. In this paper, we investigate the effect of three different feed solute mass fractions ( $w_{b0}$ ) under typical conditions for RO, as shown in Table 2.1. For the seawater feed concentration ( $w_{b0} = 0.04$ ), a higher transmembrane pressure is used than for brackish water, in order to achieve a similar permeate flux under higher osmotic pressure.

Table 2.1: Parameters used for slip velocity case study

Parameter	Value
Feed Solute Mass Fraction ( $w_{b0}$ )	0.01, 0.025, 0.04
Dimensionless Inlet Transmembrane Pressure ( $P_0 = \frac{\Delta p_{tm}}{\pi_0}$ )	1.46, 1.86, 3.65
Dimensionless Forced Slip Velocity Amplitude ( $U_{s,A} = \frac{u_{s,A}}{u_{eff}}$ )	$5.55 \times 10^{-3}$
Intrinsic Rejection ( $R$ )	0.996
Dimensionless Membrane Permeance ( $\Pi_{L_p} = \frac{L_p \pi_0}{u_{eff}}$ )	$1.98 \times 10^{-5} - 3.53 \times 10^{-3}$
Reflection Coefficient ( $\sigma$ )	1
Hydraulic Reynolds number ( $Re_h = \frac{\rho u_{eff} d_h}{\mu}$ )	408
Slip Reynolds number ( $Re_s = \frac{\rho u_{s,A} d_h}{\mu}$ )	2

## 2.4 Methodology for analysis of results

Dimensionless variables used in this paper are summarised in Table 2.2.

Table 2.2: Dimensionless variables used for this study

Dimensionless Variable	Definition
Concentration Polarisation Index ( $\gamma$ )	$w_w/w_{b0}$
Flux ( $J/J_{pure}$ )	$1 - \gamma\sigma\phi R w_{b0}/\Delta p_{tm}$
Frequency ( $F_s$ )	$f_s h_{ch}/u_{eff}$

A method typically used to estimate the peak frequency of a linear dynamic system consists of adding a stimulus to the system and carrying out frequency response analysis [26]. The frequency response is a plot of the amplitude ratio of a system output (e.g. velocity, flux, etc.) for a given input stimulus (e.g. unsteady forced slip). The frequency response plot can be calculated using a stimulus with a broad range of frequencies, such as a pulse, and dividing the Fourier transform of the observed output by the Fourier transform of the stimulus to the system. The peak frequency is the frequency at which the maximum amplitude ratio is observed, and it is termed  $F_{pl}$  in this paper. However, as the coupled hydrodynamics-mass transfer system in a spacer-filled channel is strictly non-linear, the peak frequency estimated from frequency response analysis ( $F_{pl}$ ) is not necessarily the frequency which maximises mass transfer. Nonetheless, our previous work [13] showed that  $F_{pl}$  can help approximate the actual peak frequency ( $F_{peak}$ ) for typical RO operating conditions. Therefore, this paper uses frequency response analysis to analyse the effect of membrane permeance on the peak frequency.

The analysis carried out in this paper follows the same method as [13], which uses a pulse test to determine the frequency response of  $v$ -velocity up until a cut-off frequency ( $f_{cut}$ ). The input slip velocity in dimensionless form is expressed as:

$$U_{s,pulse} = \begin{cases} 0 & , t < 0, t > t_{f_{cut}} \\ \frac{U_{s,A}}{2} \left[ 1 - \cos\left(\frac{2\pi t}{t_{f_{cut}}}\right) \right] & , 0 \leq t \leq t_{f_{cut}} \end{cases} \quad (6)$$

where:

$$t_{f_{cut}} = \frac{4}{\pi f_{cut}} \quad (7)$$

Pulse tests are carried out using transient simulations, taking as the initial state ( $t = 0$ ), a steady state solution. In addition, transient simulations with a single-frequency sinusoidal slip-velocity input are also carried out.

The time-averaged ( $\phi_{TA}$ ) and maximum ( $\phi_{max}$ ) values of spatially local variables are recorded after the convergence criteria have been met, that is, after the time-averaged variables have stabilised. The maximum value of wall shear stress ( $\bar{\tau}_{max} = \mu \left( \frac{\partial \bar{u}}{\partial y} \right)_{max}$ ) is measured because a higher wall shear stress has a greater potential to reduce membrane fouling [1]. On the other hand, global variables ( $\bar{\phi}$ ) are calculated as the area-average of the local variables along the length ( $L$ ) of the membrane region of a unit cell (spacer 7 and 8 as indicated in Figure 2.1). Global variables can therefore be expressed by:

$$\bar{\phi} = \frac{1}{L} \int \phi \, dx \quad (8)$$

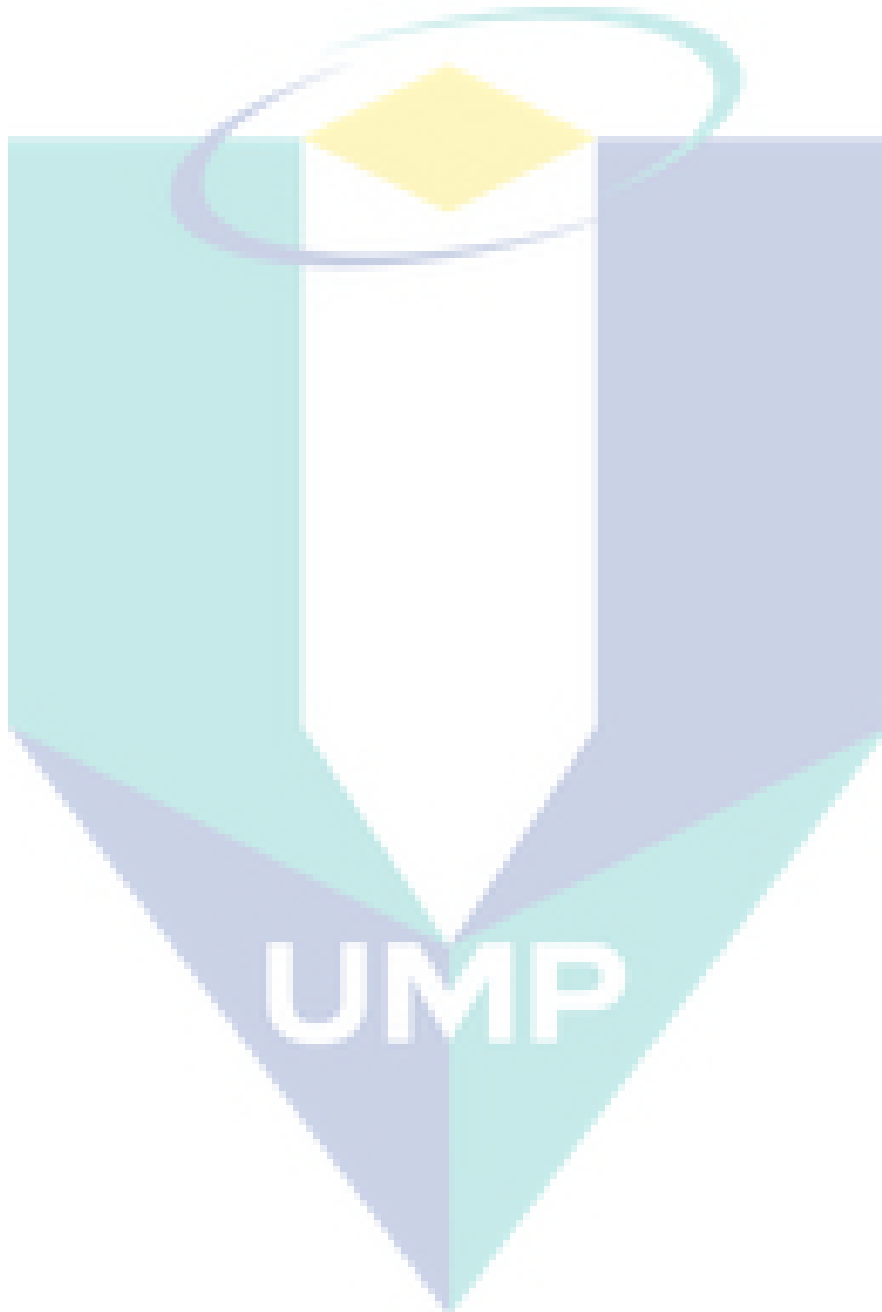
In addition, forced slip mass transfer enhancement is measured by the relative change in the concentration polarisation index [17]:

$$\tilde{\Phi} = 1 - \frac{\bar{Y}_{EO,TA}}{\bar{Y}_{NS}} = \frac{\bar{J}_{EO,TA} - \bar{J}_{NS}}{\bar{J}_{pure} - \bar{J}_{NS}} \quad (9)$$

Power number ( $Pn = Re_h^3 f_{TA}$ ) is used to measure the energy losses by comparing the pumping power at the same membrane permeance [25]. Recovery rate is determined by the

ratio of the product water flow rate ( $Q_p = L_m \bar{J}_{TA} w_{ch}$ ) to feed water flow rate ( $Q_{in} = \rho u_{b0} h_{ch} w_{ch}$ ) [27].

$$\text{Recovery rate} = \frac{L_m \bar{J}_{TA}}{\rho u_{b0} h_{ch}} \quad (10)$$



## CHAPTER 3

### RESULTS AND DISCUSSION

In order to determine the resonant frequency for forced slip velocity, a pulse test is carried out with a positive slip velocity for the whole membrane region, using different membrane permeance values. As in [13], the  $v$ -velocity is monitored during the tests at the point ‘•’ shown in Figure 3.1. After a pulse is introduced, the  $v$ -velocity oscillates with a similar pattern and magnitude for each membrane permeance. It is found that a slip velocity of 1 mm/s can induce a  $v$ -velocity of the order of 30 mm/s for a Reynolds number that is close to the transition from steady to unsteady flow, as explained in our previous work [1]. The frequency response obtained from the pulse test in slip velocity (from Figure 3.1) is shown in Figure 3.2. This figure shows similar behaviour for all of the values of membrane permeance tested, both in terms of the magnitude of the amplitude ratio and of the peak frequency ( $F_{pl} \approx 0.87$ ). This suggests that the peak frequency is very unlikely to be affected by the membrane properties and the bulk conditions, because the permeation rate is at least 7,000 times smaller than the bulk flow rate.

Figure 3.2 shows the value of the approximate peak frequency ( $F_{pl} = 0.87$ ) determined by the frequency response analysis. As the value of the  $F_{pl}$  in this study is the same as in our previous finding [17], it is expected that the value of the actual peak frequency ( $F_{peak} = 0.67$ ) determined by a single-frequency sinusoidal slip velocity in our previous finding is also the same in this study. Therefore,  $F_{peak} = 0.67$  is used in this paper to examine the effect of membrane permeance on membrane performance enhancement through slip velocity. The results of simulations using a forced slip velocity at  $F_{peak} = 0.67$ , and varying the membrane

permeance are shown in Figure 3.3, both in terms of mass transfer enhancement ( $\tilde{\Phi}$ ) and flux enhancement ( $\Delta J$ ).

As seen in Figure 3.3a, the forced slip velocity mass transfer enhancement factor ( $\tilde{\Phi}$ ) reaches a maximum at a membrane permeance of  $9.87 \times 10^{-12} \text{ m s}^{-1} \text{ Pa}^{-1}$  for all feed bulk concentrations ( $w_{b0}$ ) tested. The maximum in  $\tilde{\Phi}$  indicates that the highest effectiveness for concentration polarisation reduction is in the mid-range of membrane permeance values typically used for brackish water, and is related to the competing effect between flux ratios ( $\bar{J}_{EO}/\bar{J}_{pure}$  and  $\bar{J}_{NS}/\bar{J}_{pure}$ ) in equation (9). At a lower membrane permeance,  $\tilde{\Phi}$  increases because  $\tilde{\Phi}$  is dominated by the difference between  $\bar{J}_{EO,TA}$  and  $\bar{J}_{NS}$  as the difference between  $\bar{J}_{pure}$  and  $\bar{J}_{NS}$  is smaller. However, at a higher membrane permeance,  $\tilde{\Phi}$  decreases because  $\bar{J}_{pure}$  is much larger than  $\bar{J}_{NS}$  as both  $\bar{J}_{EO,TA}$  and  $\bar{J}_{NS}$  approach a constant value. This suggests that at higher feed concentration there is lower flux, which leads to lower concentration polarisation and thus lower mass transfer enhancement. Therefore, at lower CP there is less room for improvement.

UMP

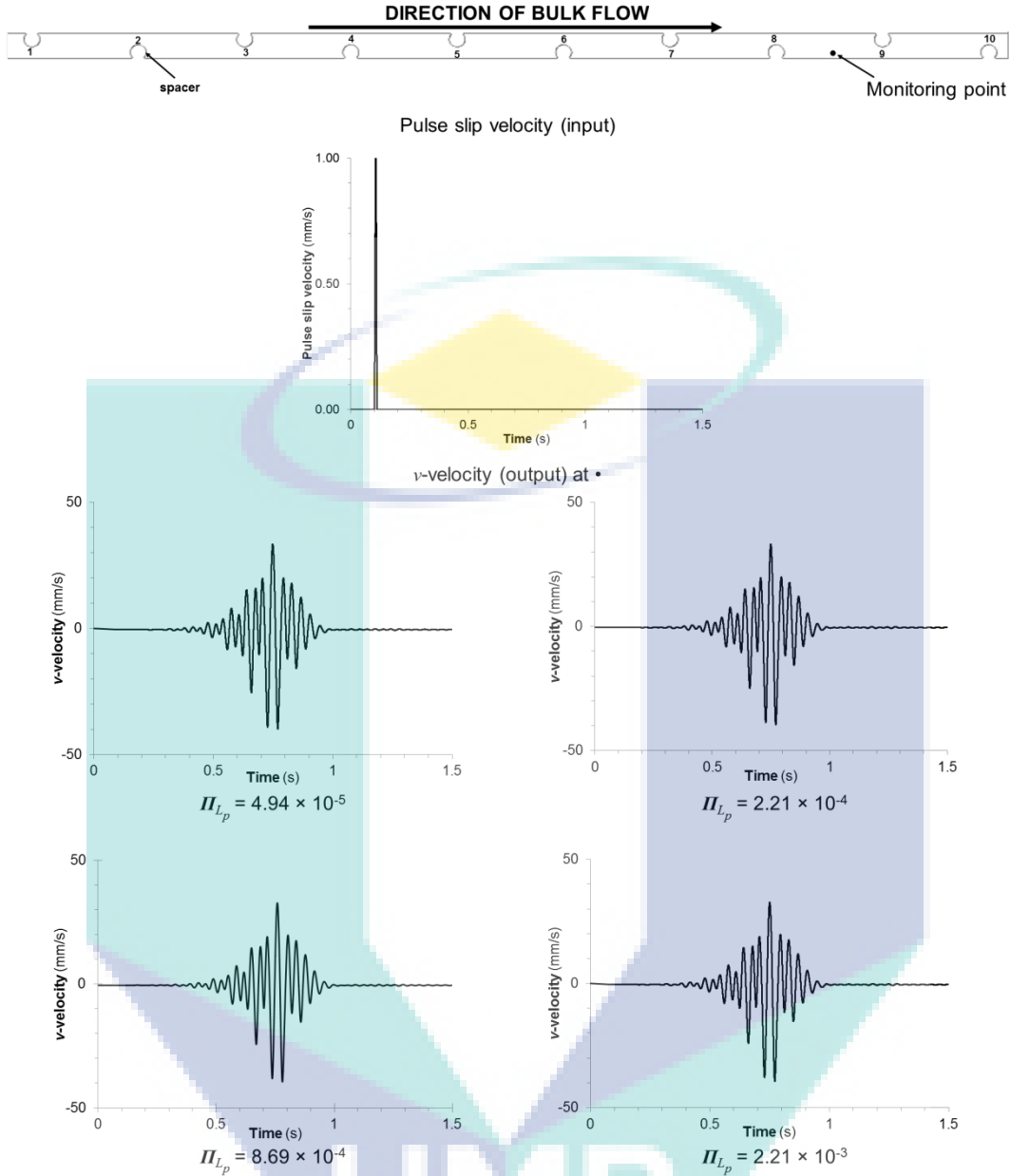


Figure 3.1: Frequency response time data for the pulse slip velocity and corresponding  $v$ -velocity at monitoring point '•' (located at one third of the channel height from the bottom membrane surface), for  $\Pi_{L_p} = 4.94 \times 10^{-5}$ ,  $2.21 \times 10^{-4}$ ,  $8.69 \times 10^{-4}$  and  $2.21 \times 10^{-3}$  at the same feed bulk concentration ( $w_{b0} = 0.025$ ) and  $Re = 408$ .

Although Figure 3.3a shows a peak in  $\tilde{\Phi}$  at the mid-range brackish water membrane permeance, Figure 3.3b shows that at the high end of membrane permeance tested ( $\Pi_{L_p} > 10^{-4}$  or  $L_p > 10^{-11} \text{ m s}^{-1} \text{ Pa}^{-1}$ ), the tendency for forced slip to further increase the permeate flux (and recovery rate) is weaker but does not disappear. This appears to be the case for all  $\omega_{b0}$

values tested. At the largest permeance simulated, the flux was found to increase roughly 23 % due to forced slip, which is significantly higher than the flux increase of around 13 % at the peak in  $\tilde{\Phi}$ . This is because at a higher permeance, CP is larger and thus the effectiveness of forced slip velocity in enhancing mixing increases, but not at the linear rate at which  $J_{pure}$  increases due to a larger  $L_p$ . Comparing the effect of permeance on flux enhancement against the results from one of our previous studies [17], it is clear that steady forced-slip shows less flux enhancement than unsteady forced-slip (about 11 % flux increase at the highest permeance tested,  $L_p \sim 3.95 \times 10^{-10} \text{ m s}^{-1} \text{ Pa}^{-1}$ ). However, the results agree in the sense that a larger increase in permeate flux occurs at a higher membrane permeance despite the decrease in  $\tilde{\Phi}$ . This means that forced-slip flux enhancement at higher membrane permeance is independent of whether steady or unsteady slip velocity is implemented, and the decrease in  $\tilde{\Phi}$  can be explained by the linear increase of  $J_{pure}$  as membrane permeance increases.

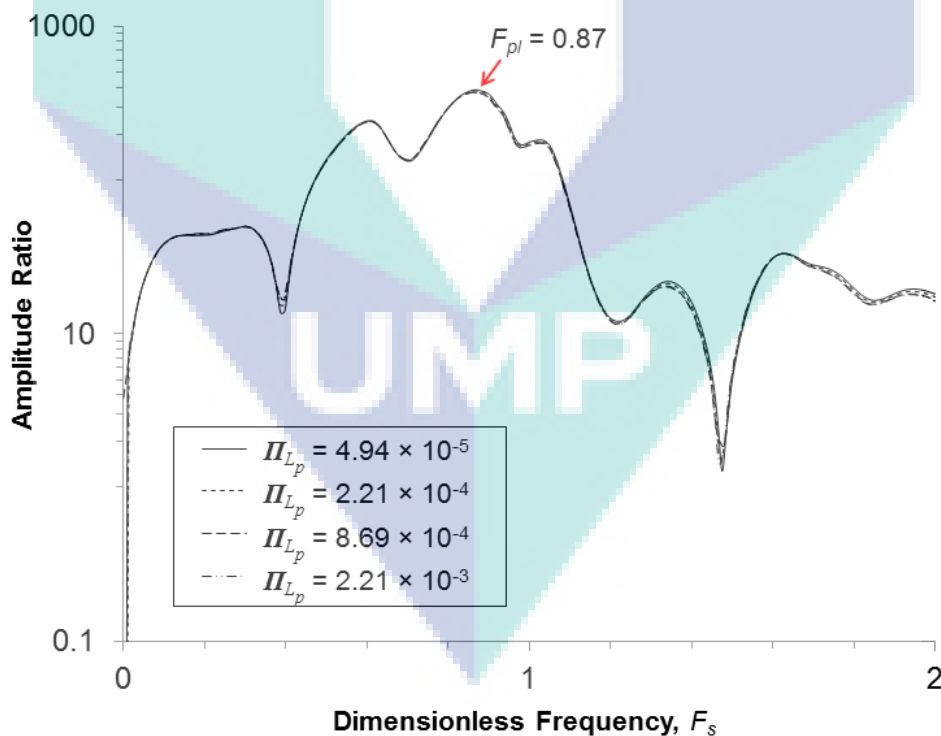


Figure 3.2: Frequency response of  $v$ -velocity at location ‘•’ to a pulse in slip velocity for  $\Pi_{L_p} = 4.94 \times 10^{-5}$ ,  $2.21 \times 10^{-4}$ ,  $8.69 \times 10^{-4}$  and  $2.21 \times 10^{-3}$  at the same feed solute concentration ( $w_{b0} = 0.025$ ) and  $Re = 408$ .

Figure 3.4 shows the effect of slip velocity applied at  $F_{peak}$  on the velocity field and solute concentration, in the region downstream of spacer 8 for the lowest ( $\Pi_{L_p} = 4.94 \times 10^{-5}$ ) and the highest ( $\Pi_{L_p} = 2.21 \times 10^{-3}$ ) membrane permeance values considered. The figure shows that when there is no slip velocity, the solute concentration near the wall for the high end of the membrane permeance ( $\Pi_{L_p} = 2.21 \times 10^{-3}$ ) is significantly larger than that of the low end of the membrane permeance ( $\Pi_{L_p} = 4.94 \times 10^{-5}$ ). However, when a forced slip velocity is applied at the  $F_{peak}$ , vortex shedding occurs and there is a similar effect on mass transfer for both high and low end of membrane permeance. This indicates that mass transfer is greatly enhanced by the unsteady effect, particularly due to the occurrence of vortex shedding.

Figure 3.5 shows the results in terms of friction and energy losses for the systems simulated. From Figure 3.5a, it is evident that the forced slip velocity leads to more than a two-fold increase in maximum shear stress ( $\bar{\tau}_{max}$ ) relative to the case without a forced slip velocity, hence indicating the potential for fouling reduction using forced slip. Moreover, membrane permeance has a negligible effect on maximum shear stress under forced slip, with only a 1.8% decrease as permeance increases over 2 orders of magnitude. This slight decrease in maximum shear stress is attributed to the increase in permeate flux as the membrane permeance increases, thus causing a decrease in velocity near the membrane wall. Moreover, Figure 3.5b shows that the pumping energy requirements under forced slip for all  $L_p$  and  $w_{b0}$  values explored present a slight increase of 5–7 % from the case without forced slip at the same Reynolds number of 408, due to the induction of vortex shedding [13]. It should be noted that the energy required to induce vortex shedding depends on the type of flow perturbation approach used.

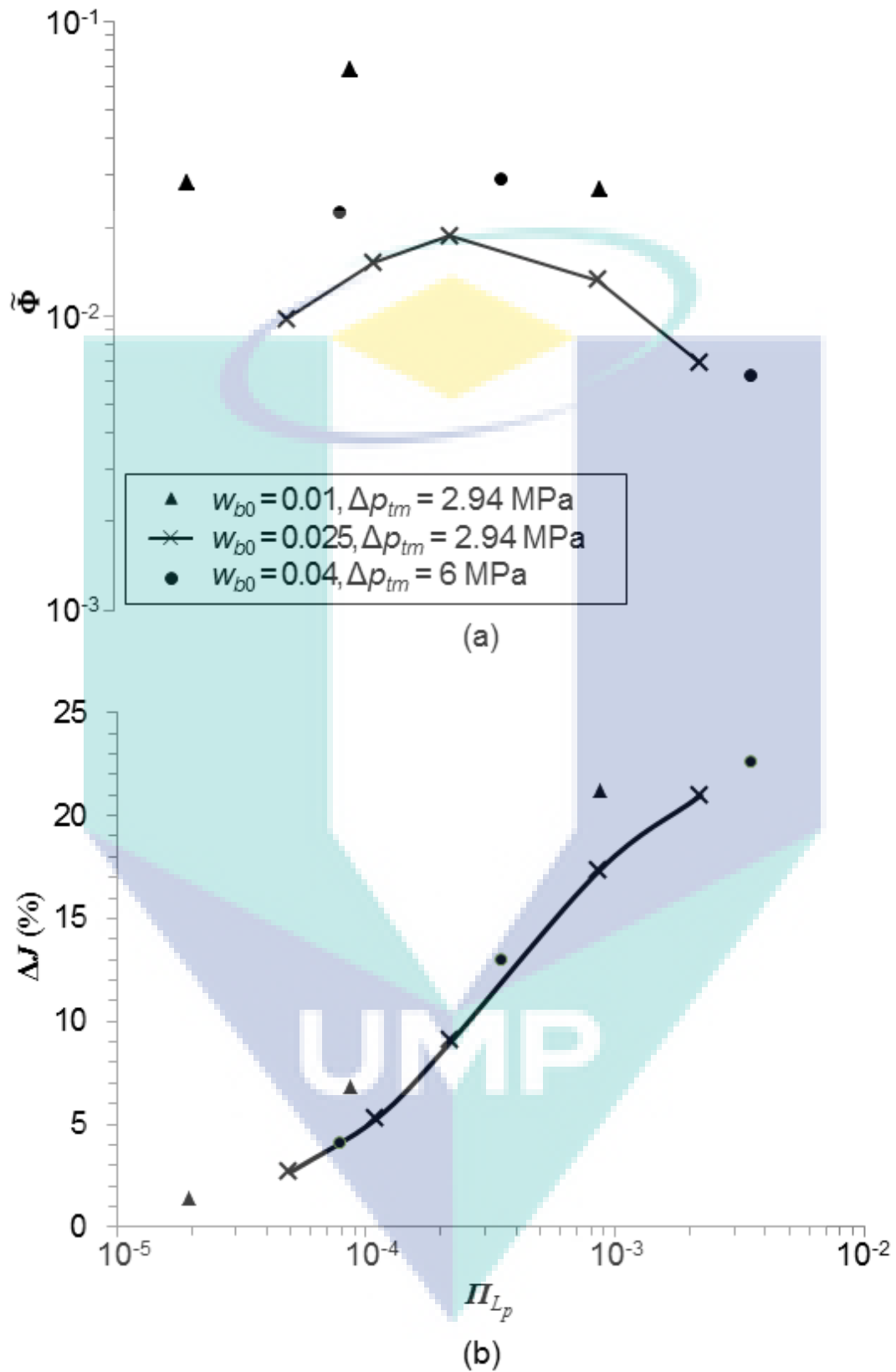
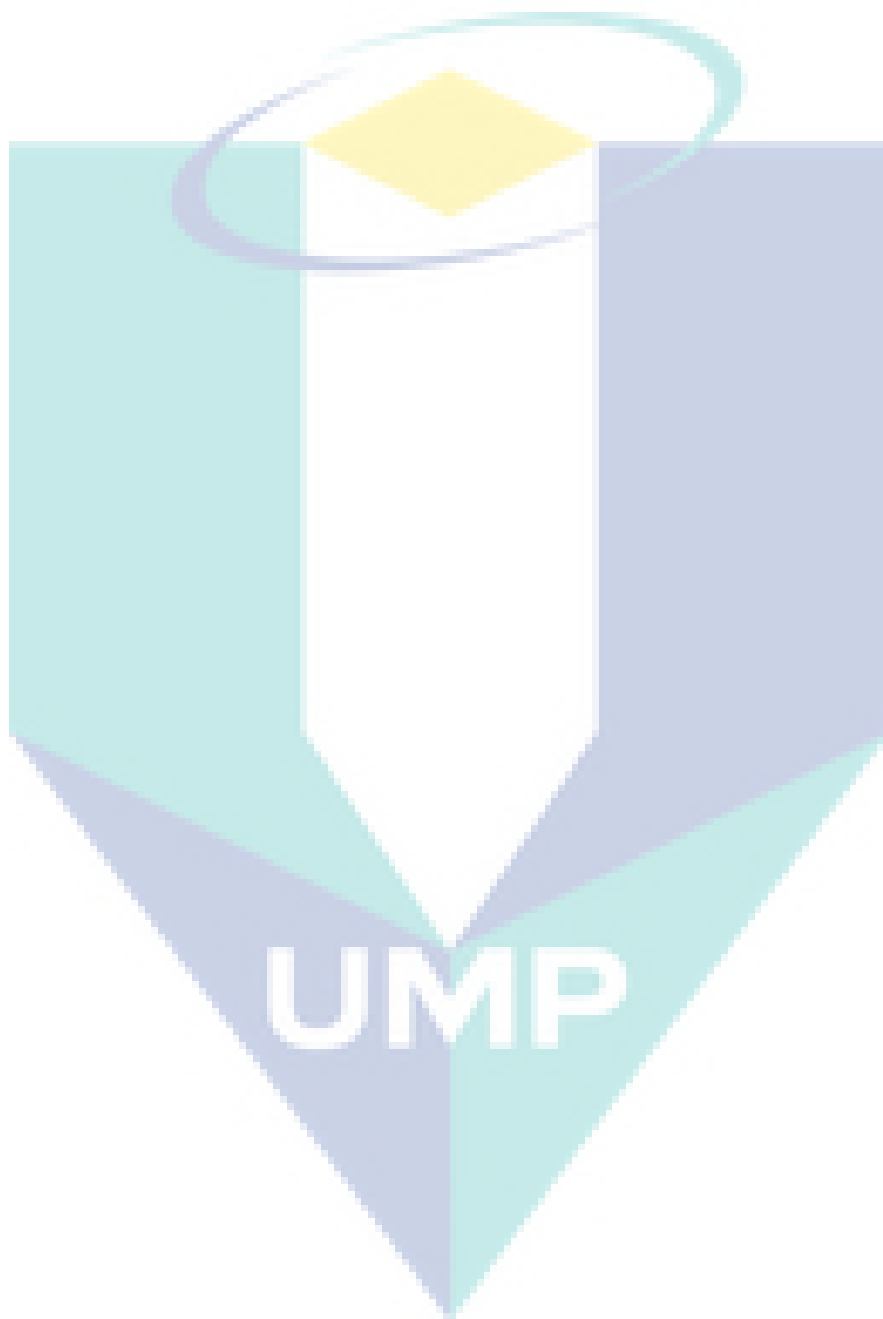


Figure 3.3: Effect of membrane permeance on (a) forced slip velocity mass transfer enhancement and (b) relative change in permeate flux at different inlet solute concentration ( $w_{b0}$ ) of 0.01 ( $\Delta p_{tm} = 2.94$  MPa), 0.025 ( $\Delta p_{tm} = 2.94$  MPa) and 0.04 ( $\Delta p_{tm} = 6$  MPa) for  $Re = 408$ .



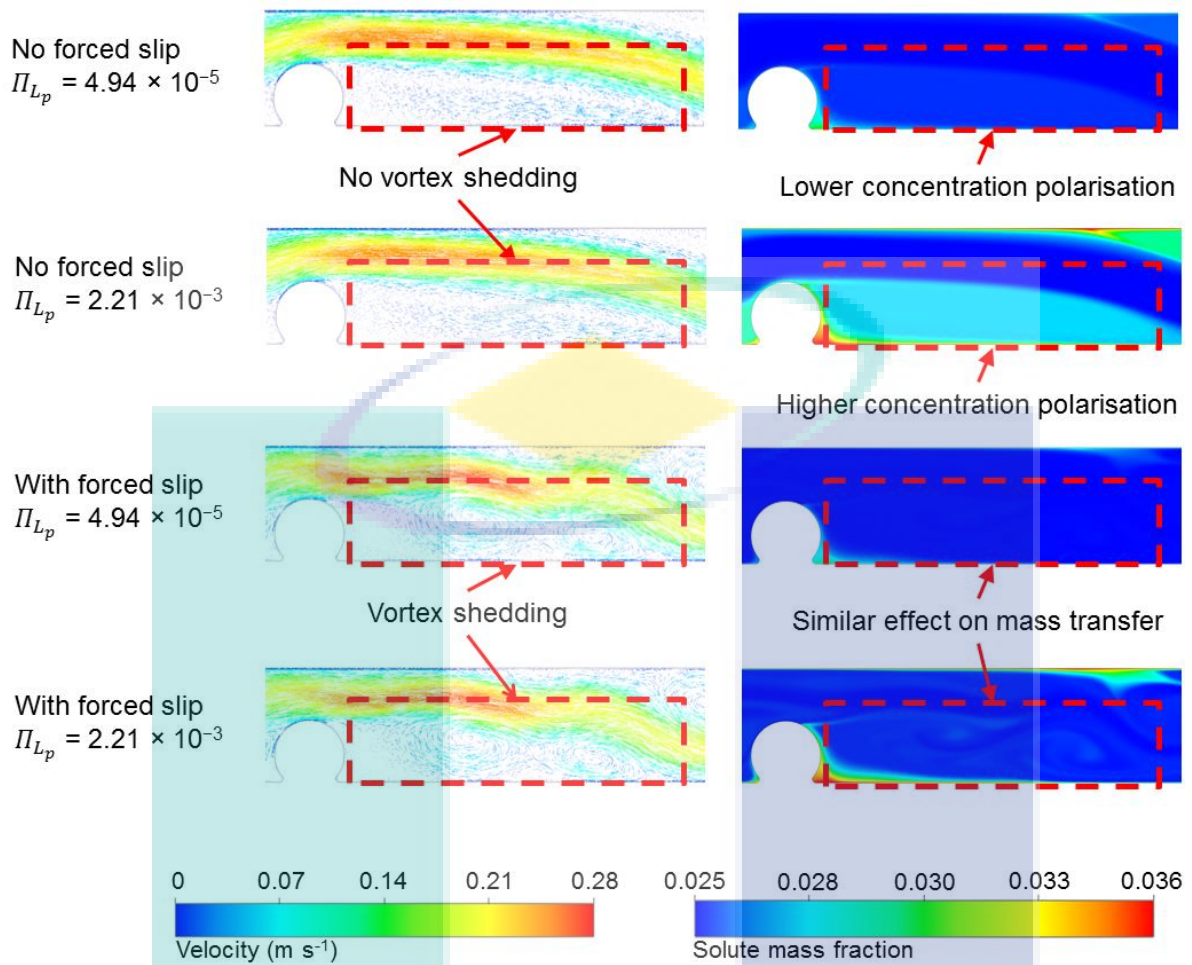


Figure 3.4: Effect of slip velocity applied at the  $F_{peak}$  on the velocity field and solute concentration in the region within spacer 8 for  $\Pi_{L_p} = 4.94 \times 10^{-5}$  and  $2.21 \times 10^{-3}$  at the same feed solute concentration ( $w_{b0} = 0.025$ ) and  $Re = 408$ .

UMP

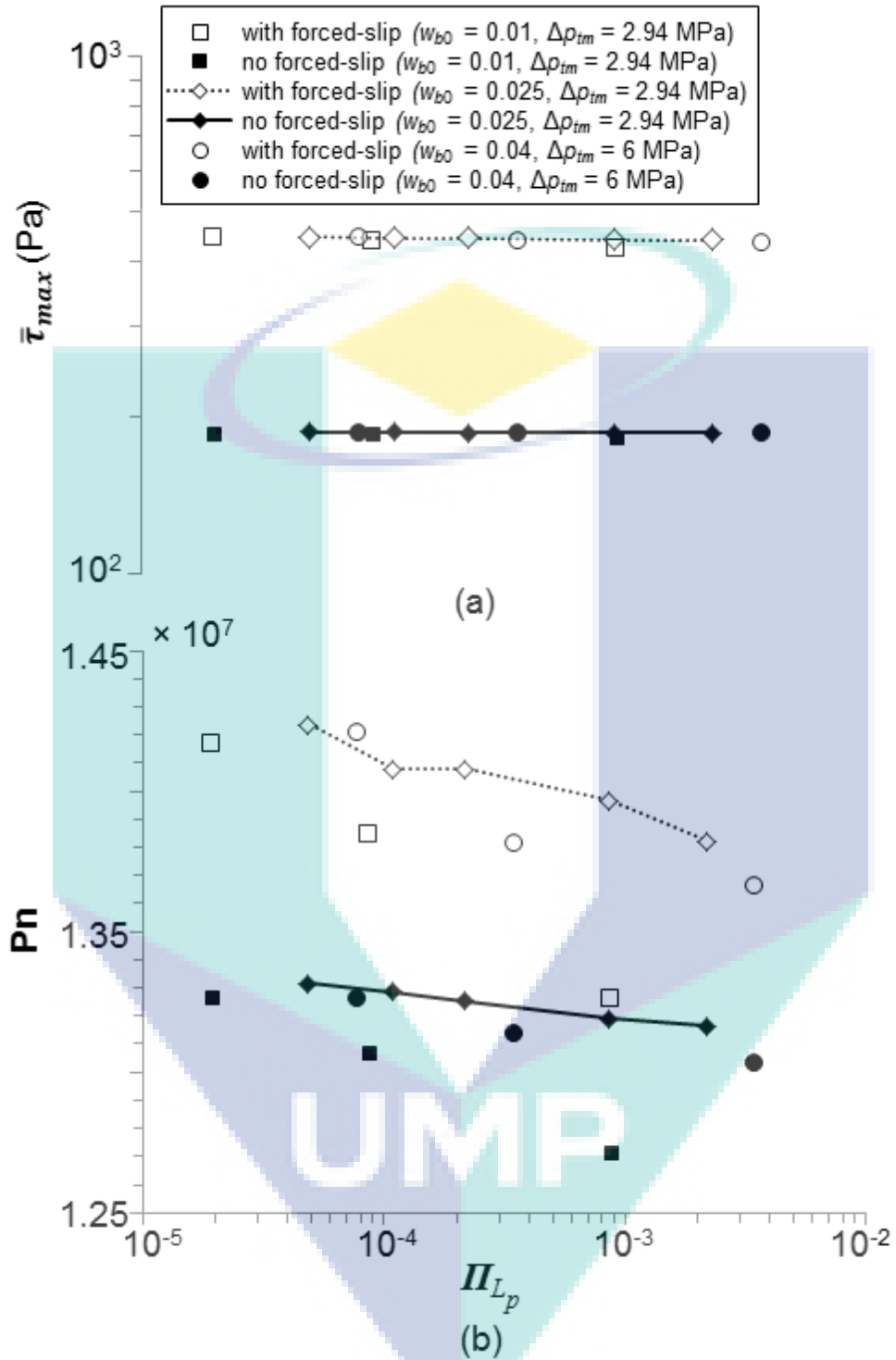


Figure 3.5: Effect of membrane permeance on (a) maximum shear stress and (b) Power number at three different values of  $w_{b0}$ : 0.01 ( $\Delta p_{tm} = 2.94$  MPa), 0.025 ( $\Delta p_{tm} = 2.94$  MPa) and 0.04 ( $\Delta p_{tm} = 6$  MPa) for  $Re = 408$ .

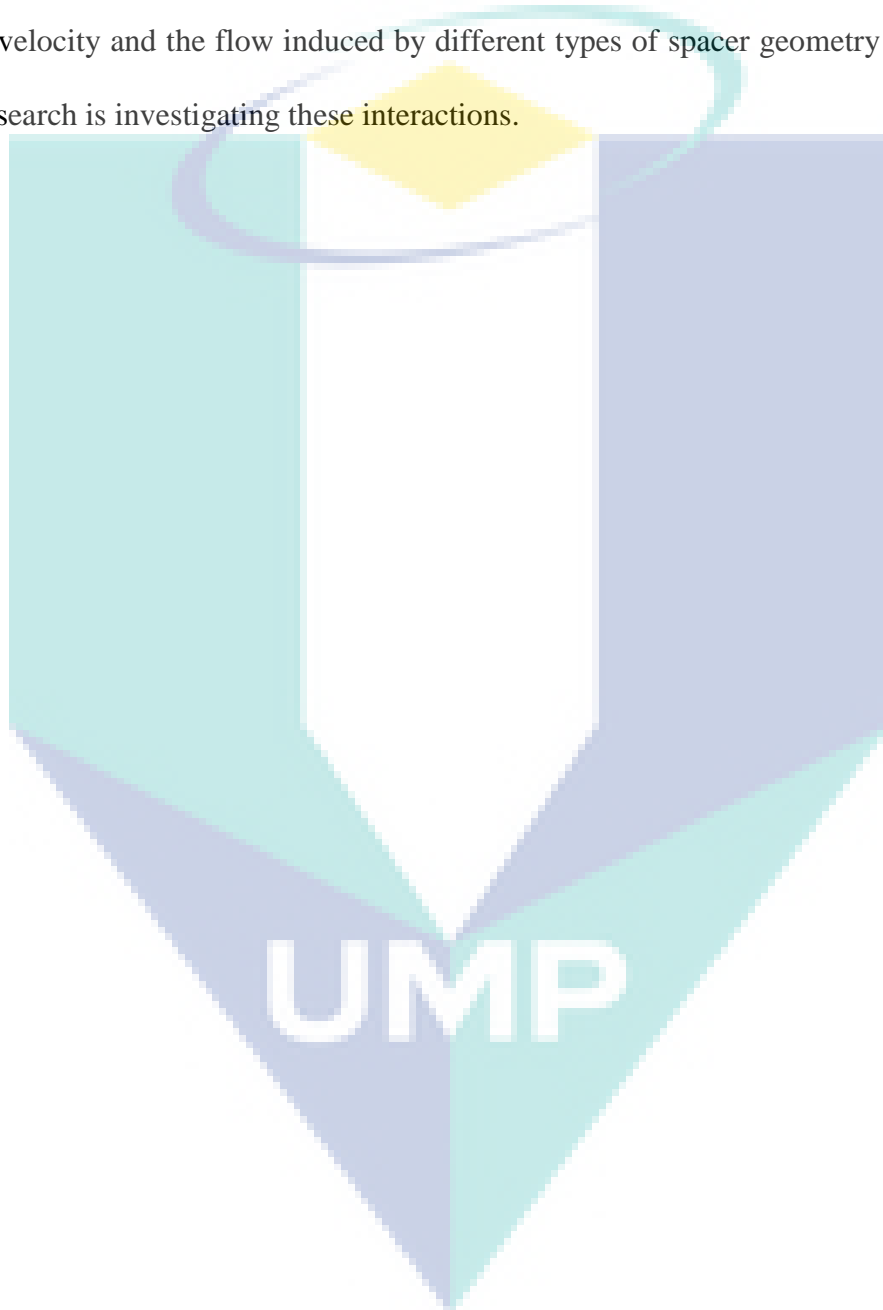
## CHAPTER 4

### CONCLUSION AND RECOMMENDATIONS

The results in this paper show that the peak frequency for unsteady forced slip is not affected by the membrane permeance. This is because the magnitude of membrane permeation is relatively insignificant compared with the magnitude of the bulk flow velocity, even at a higher permeance. Although the peak in mass transfer enhancement factor ( $\tilde{\Phi}$ ) indicates that reduction of concentration polarisation is most effective for membrane permeance in the range typically used for brackish water, permeate flux and recovery rate can still be significantly enhanced (by up to 23 %) for higher values of membrane permeance, at the expense of slightly higher (5–7 %) pumping energy requirements. Furthermore, the results show that at any membrane permeance, forced slip can improve the maximum shear stress ( $\bar{\tau}_{max}$ ) by at least 130 %, thereby reducing the effects of fouling. Overall the results show that forced slip velocity is more effective at a higher operating flux.

Although this paper only studies the effect of unsteady forced slip velocity in the vicinity of boundary layer, other hydrodynamic perturbation (forced transients) methods can also be used to affect the flow in the membrane boundary layer and improve mass transfer when applied at the resonant frequency. This is because when a flow perturbation is applied at the resonant frequency, it has the potential to induce vortex shedding which results in a greater mixing and mass transfer enhancement. The results presented in this paper suggest that the permeance of typical membranes used for brackish water treatment should not affect the value of the resonant frequency.

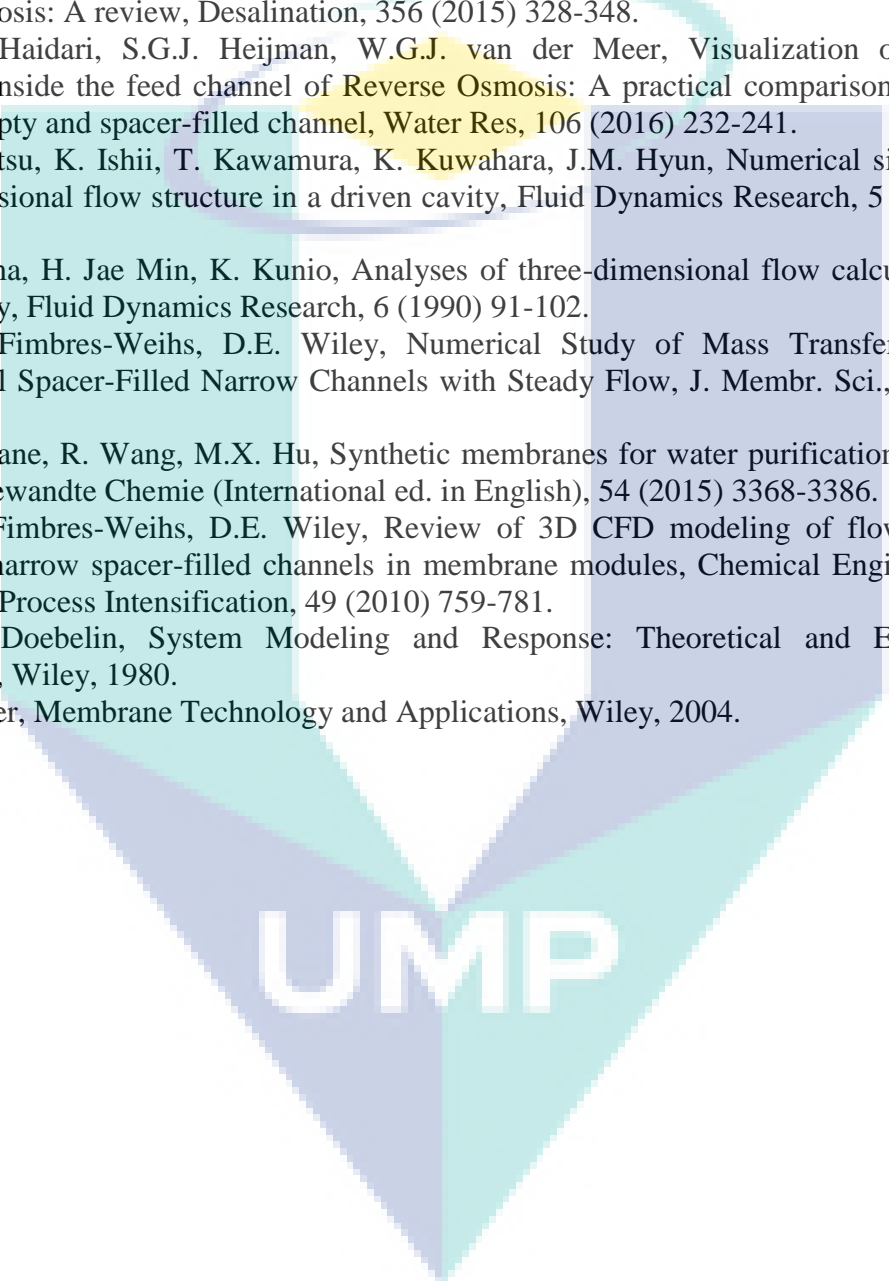
We investigated the effect of membrane permeance on the resonant frequency, mass transfer and flux enhancement when using an unsteady forced slip velocity for a single type of spacer geometry. As the bulk flow characteristics will likely change for different spacer geometries, it may be possible to further enhance mass transfer if the interaction between the forced slip velocity and the flow induced by different types of spacer geometry is optimised. Ongoing research is investigating these interactions.



## REFERENCES

- [1] Y.Y. Liang, G. Fimbres Weihs, R. Setiawan, D. Wiley, CFD modelling of unsteady electro-osmotic permeate flux enhancement in membrane systems, *Chemical Engineering Science*, 146 (2016) 189-198.
- [2] P.L.T. Brian, Concentration Polarization in Reverse Osmosis Desalination with Variable Flux and Incomplete Salt Rejection, *Industrial & Engineering Chemistry Fundamentals*, 4 (1965) 439-445.
- [3] E. Matthiasson, B. Sivik, Concentration polarization and fouling, *Desalination*, 35 (1980) 59-103.
- [4] R.A. Shaw, R. Deluca, W.N. Gill, Reverse osmosis: increased productivity by reduction of concentration polarization in laminar flow reverse osmosis using intermediate non-rejecting membrane sections, *Desalination*, 11 (1972) 189-205.
- [5] T.K. Sherwood, P.L.T. Brian, R.E. Fisher, L. Dresner, Salt Concentration at Phase Boundaries in Desalination by Reverse Osmosis, *Industrial & Engineering Chemistry Fundamentals*, 4 (1965) 113-118.
- [6] D. Cohen-Tanugi, J.C. Grossman, Water Desalination across Nanoporous Graphene, *Nano Letters*, 12 (2012) 3602-3608.
- [7] D. Cohen-Tanugi, R.K. McGovern, S.H. Dave, J.H. Lienhard, J.C. Grossman, Quantifying the potential of ultra-permeable membranes for water desalination, *Energy & Environmental Science*, 7 (2014) 1134-1141.
- [8] A. Alexiadis, D.E. Wiley, D.F. Fletcher, J. Bao, Laminar Flow Transitions in a 2D Channel with Circular Spacers, *Industrial & Engineering Chemistry Research*, 46 (2007) 5387-5396.
- [9] A.J. Karabelas, Key issues for improving the design and operation of spiral-wound membrane modules in desalination plants, *Desalination and Water Treatment*, 52 (2013) 1820-1832.
- [10] A.J. Karabelas, M. Kostoglou, C.P. Koutsou, Modeling of spiral wound membrane desalination modules and plants – review and research priorities, *Desalination*, 356 (2015) 165-186.
- [11] X. Yang, H. Yu, R. Wang, A.G. Fane, Analysis of the effect of turbulence promoters in hollow fiber membrane distillation modules by computational fluid dynamic (CFD) simulations, *Journal of Membrane Science*, 415–416 (2012) 758-769.
- [12] C. Rodrigues, V. Geraldes, M.N. de Pinho, V. Semião, Mass-transfer entrance effects in narrow rectangular channels with ribbed walls or mesh-type spacers, *Chemical Engineering Science*, 78 (2012) 38-45.
- [13] Y.Y. Liang, G.A. Fimbres Weihs, D.E. Wiley, CFD modelling of electro-osmotic permeate flux enhancement in spacer-filled membrane channels, *Journal of Membrane Science*, 507 (2016) 107-118.
- [14] J. Jurado, B.J. Bellhouse, Application of electric fields and vortex mixing for enhanced ultrafiltration, *Filtration & Separation*, 31 (1994) 273-268.
- [15] G.A. Fimbres-Weihs, J. Álvarez-Sánchez, Synergies Between Pulsatile Flow and Spacer Filaments in Reverse Osmosis Modules, in: A. Maciel-Cerda (Ed.) *Membranes: Materials, Simulations, and Applications*, Springer International Publishing, Cham, 2017, pp. 67-75.
- [16] W. Li, X. Su, A. Palazzolo, S. Ahmed, E. Thomas, Reverse osmosis membrane, seawater desalination with vibration assisted reduced inorganic fouling, *Desalination*, 417 (2017) 102-114.

- [17] Y.Y. Liang, M.B. Chapman, G.A. Fimbres Weihs, D.E. Wiley, CFD modelling of electro-osmotic permeate flux enhancement on the feed side of a membrane module, *J. Membr. Sci.*, 470 (2014) 378-388.
- [18] Y.Y. Liang, G.A. Fimbres Weihs, D.E. Wiley, Approximation for modelling electro-osmotic mixing in the boundary layer of membrane systems, *J. Membr. Sci.*, 450 (2014) 18-27.
- [19] F. Zamani, J.W. Chew, E. Akhondi, W.B. Krantz, A.G. Fane, Unsteady-state shear strategies to enhance mass-transfer for the implementation of ultrapermeable membranes in reverse osmosis: A review, *Desalination*, 356 (2015) 328-348.
- [20] A.H. Haidari, S.G.J. Heijman, W.G.J. van der Meer, Visualization of hydraulic conditions inside the feed channel of Reverse Osmosis: A practical comparison of velocity between empty and spacer-filled channel, *Water Res.*, 106 (2016) 232-241.
- [21] R. Iwatsu, K. Ishii, T. Kawamura, K. Kuwahara, J.M. Hyun, Numerical simulation of three-dimensional flow structure in a driven cavity, *Fluid Dynamics Research*, 5 (1989) 173-189.
- [22] I. Reima, H. Jae Min, K. Kunio, Analyses of three-dimensional flow calculations in a driven cavity, *Fluid Dynamics Research*, 6 (1990) 91-102.
- [23] G.A. Fimbres-Weihs, D.E. Wiley, Numerical Study of Mass Transfer in Three-Dimensional Spacer-Filled Narrow Channels with Steady Flow, *J. Membr. Sci.*, 306 (2007) 228-243.
- [24] A.G. Fane, R. Wang, M.X. Hu, Synthetic membranes for water purification: status and future, *Angewandte Chemie (International ed. in English)*, 54 (2015) 3368-3386.
- [25] G.A. Fimbres-Weihs, D.E. Wiley, Review of 3D CFD modeling of flow and mass transfer in narrow spacer-filled channels in membrane modules, *Chemical Engineering and Processing: Process Intensification*, 49 (2010) 759-781.
- [26] E.O. Doebelin, *System Modeling and Response: Theoretical and Experimental Approaches*, Wiley, 1980.
- [27] R. Baker, *Membrane Technology and Applications*, Wiley, 2004.

The logo for UMP (Universitas Muhammadiyah Purwokerto) is a large, stylized letter 'U' composed of several overlapping triangles in shades of blue and teal. The letters 'UMP' are printed in white, bold, sans-serif font across the center of the 'U' shape.

UMP